ASR-9 Refractivity Measurements Using Ground Targets

J.Y.N. Cho

13 November 2006

Lincoln Laboratory

MASSACHUSETTS INSTITUTE OF TECHNOLOGY

LEXINGTON, MASSACHUSETTS

1. Report No. ATC-328	2. Government Accession No.	3. Recipient's Catalog No.
4. Title and Subtitle **ASR-9 Refractivity Measurements Using Ground Targets**		5. Report Date **13 November 2006**
		6. Performing Organization Code
7. Author(s) **John Y.N. Cho**		8. Performing Organization Report No. **ATC-328**
9. Performing Organization Name and Address **MIT Lincoln Laboratory** **244 Wood Street** **Lexington, MA 02420-9108**		10. Work Unit No. (TRAIS)
		11. Contract or Grant No. **FA8721-05-C-0002**
12. Sponsoring Agency Name and Address **Department of Transportation** **Federal Aviation Administration** **800 Independence Ave., S.W.** **Washington, DC 20591**		13. Type of Report and Period Covered **Project Report**
		14. Sponsoring Agency Code

15. Supplementary Notes

This report is based on studies performed at Lincoln Laboratory, a center for research operated by Massachusetts Institute of Technology, under Air Force Contract FA8721-05-C-0002.

16. Abstract

Weather radars rely on the presence of radiowave scattering entities such as hydrometeors and insects to sense the dynamic evolution of the atmosphere. Under clear-air, low-reflectivity conditions, when no such "visible" tracers are present, air mass boundaries such as the outflow edge of a dry microburst may go undetected.

Recently, a radar data processing technique was developed to estimate the near-ground atmospheric refractivity field using ground targets. Refractivity is dependent on the moist thermodynamic variables of the atmosphere and, thus, can be used to detect air mass changes and boundaries. In this study, we apply this technique for the first time to ASR-9 WSP data. Comparisons with measurements from a meteorological station show good consistency. The potential exists for improving the poor dry-site performance of the current WSP microburst detector by adding interest information provided by the estimated refractivity field.

Adequate computational power is the sole requirement for implementing this scheme; aside from that no alteration or addition is necessary to the ASR-9 hardware. Its primary weaknesses are the limited range of coverage (~20 km) and the sensitivity to vertical variation in refractivity and variance of target height. Also, further testing is needed during more appropriate meteorological conditions to prove that dry wind-shear events can really be detected in the derived refractivity field.

17. Key Words	18. Distribution Statement **This document is available to the public through the National Technical Information Service, Springfield, VA 22161.**

19. Security Classif. (of this report) **Unclassified**	20. Security Classif. (of this page) **Unclassified**	21. No. of Pages **44**	22. Price

FORM DOT F 1700.7 (8-72)   Reproduction of completed page authorized

EXECUTIVE SUMMARY

Weather radars rely on the presence of radiowave scattering entities such as hydrometeors and insects to sense the dynamic evolution of the atmosphere. Under clear-air, low-reflectivity conditions, when no such "visible" tracers are present, air mass boundaries such as the outflow edge of a dry microburst may go undetected.

Recently, a radar data processing technique was developed to estimate the near-ground atmospheric refractivity field using ground targets. Refractivity is dependent on the moist thermodynamic variables of the atmosphere and, thus, can be used to detect air mass changes and boundaries. In this study, we apply this technique for the first time to Airport Surveillance Radar-9 (ASR-9) Weather Systems Processor (WSP) data. Comparisons with measurements from a meteorological station show good consistency. The potential exists for improving the capability of the WSP to detect low-reflectivity wind-shear phenomena by adding interest information provided by the estimated refractivity field.

Adequate computational power is the sole requirement for implementing this scheme—aside from that, no alteration or addition is necessary to the ASR-9 hardware. Its primary weakness is the sensitivity to vertical variation in refractivity and variance of target height. It also has a limited range of coverage (~20 km), but that is acceptable for terminal-area coverage. Further testing is needed during more appropriate meteorological conditions and at other sites to prove that dry wind-shear events can really be detected in the derived refractivity field by this class of radar, and that the technique is robust under various topographical settings.

ACKNOWLEDGMENTS

TABLE OF CONTENTS

Page

LIST OF ILLUSTRATIONS

LIST OF TABLES

1. INTRODUCTION

Knowledge of the spatial and temporal variability of near-surface humidity is a key to improving convective initiation forecasts. Its mapping would also allow detection of a dry microburst outflow propagating in a low-reflectivity environment that is difficult to sense with weather radars. Thus, for weather monitoring and forecasting in the service of aviation safety and operational efficiency, the near-surface humidity field is extremely important, and yet coverage of this parameter is still rather sparse.

Building a dense network of *in situ* sensors is one way to alleviate the sampling problem. For dry wind-shear phenomena, supplementing the weather radar with a Doppler lidar could effectively fill in the observational gap (Keohan et al. 2006). Both strategies require new hardware and support infrastructure, which lead to substantial cost. Global Positioning System (GPS) measurements do not provide fine vertical resolution and are unreliable near the surface (Braun 2001). An alternative (or supplementary) technique is to utilize data gathered by operational weather radars in a new way, i.e., deriving the refractivity field from phase measurements of ground targets. The obvious advantage of this approach is that only additional computational time is required to produce the new product, i.e., its implementation cost is low. Experiments have shown that the technique works well on S-band radars (Fabry et al. 1997; Weckwerth et al. 2005; Cheong et al. 2005). For airport weather services, there may be great benefit realized if it could be applied to operational systems such as the Federal Aviation Administration's (FAA) Airport Surveillance Radar-9 (ASR-9) Weather Systems Processor (WSP) (Weber and Stone 1995; Evans and Weber 2000), which is an S-band system. On a national scale, inclusion of all FAA aircraft surveillance radars (132 ASR-9s, 101 ASR-11s, and 101 Air Route Surveillance Radars (ARSRs)) to the proposed application of refractivity measurements by the Weather Surveillance Radar-1988 Doppler (WSR-88D) network would greatly increase the coverage of near-surface humidity observations. This report describes the first application of this novel physical principle to data collected by an ASR-9 WSP. We briefly summarize the methodology, then present initial results.

2. REFRACTIVITY MEASUREMENT

2.1 THEORY

Classically, radars transmit a signal, and the returned signal from the target of choice is processed for power and sometimes Doppler spectral parameters to derive estimate quantities of interest. This basic procedure (or at least the principle) has not changed since the advent of the radar. Even polarization diversity, which is just now about to be put into operational use in weather radars, was known and intensively studied in the early days of radar (1940s and 1950s). In the latter half of the 20th century, radar development has been more about advances in hardware technology and signal processing technique than any fundamental changes or additions to the physical principle of Doppler detection. Refractivity measurement via ground clutter targets (Fabry et al. 1997) is a rare example of the Doppler radar being utilized in a manner that is significantly different from the classical mode.

Ground target signals are normally considered to be nuisances to be avoided, "clutter" mixed with the desired signal from weather targets. Ground targets, however, can be stationary, making them good references. The round-trip travel time of a transmitted pulse reflected back by the target to the radar is

$$t_{\text{travel}} = 2r\frac{n}{c} \; , \tag{1}$$

where r is range to target, c is the speed of light in vacuum, and n is the refractive index of the propagation medium. Thus, if t_{travel} can be measured accurately enough, temporal changes in n can be computed. This can be related to the phase given by

$$\phi(r) = 2\pi f t_{\text{travel}} = \frac{4\pi f}{c}\int_0^r n(r',t)dr' \; , \tag{2}$$

where f is the radar frequency. In practice, the phase change

$$\Delta\phi(r,t) = \phi(r,t) - \phi(r,t_{\text{ref}}) = \frac{4\pi f}{c}\int_0^r [n(r',t) - n(r',t_{\text{ref}})]dr' \; , \tag{3}$$

is measured, where the reference measurement is made at a time when the refractive index field is uniform over the spatial domain of interest. Note that this quantity is integrated over space. In order to derive local quantities we can perform a spatial derivative on (3) to yield

$$\Delta n(r,t) = \frac{c}{4\pi f}\frac{d}{dr}\Delta\phi(r,t) \quad . \tag{4}$$

Because the changes are quite small, the results are usually presented in terms of changes in the refractivity given by

$$\Delta N(r,t) = 10^6 \Delta n(r,t) \quad . \tag{5}$$

In a clear atmosphere devoid of solid and liquid particles and objects, the refractivity can be related to the thermodynamic variables as (Bean and Dutton 1968)

$$N = 77.6\frac{p}{T} + 3.73\times10^5\frac{e}{T^2} \quad , \tag{6}$$

where p is pressure (hPa), T is temperature (K), and e is the water vapor pressure (hPa). Refractivity is therefore not a direct measure of humidity. Figure 1 shows the dependence of N on temperature and relative humidity. At temperatures significantly below freezing, the dependence on humidity is very weak, whereas at warm temperatures humidity change dominates the refractivity variation. We see that refractivity becomes a better proxy of relative humidity at warmer temperatures.

2.2   PRACTICAL PROCEDURE

The above exposition briefly outlined the basic refractivity measurement concept in an ideal environment. There are a number of issues, however, that introduce additional difficulty in practice. The following procedure used for computation of the refractivity change field is adapted from Fabry (2004).

Ground targets are not necessarily stationary. Even objects such as trees that we normally think of as stationary have leaves and branches that flutter and sway in the wind. Since the wavelength of weather radars is only centimeters long, such motions often generate phase changes that are a substantial fraction of 2π or more. Power lines, street signs, stop lights, and exhaust vents can all fluctuate in position. Clearly some metric is needed to filter out unsuitable targets.
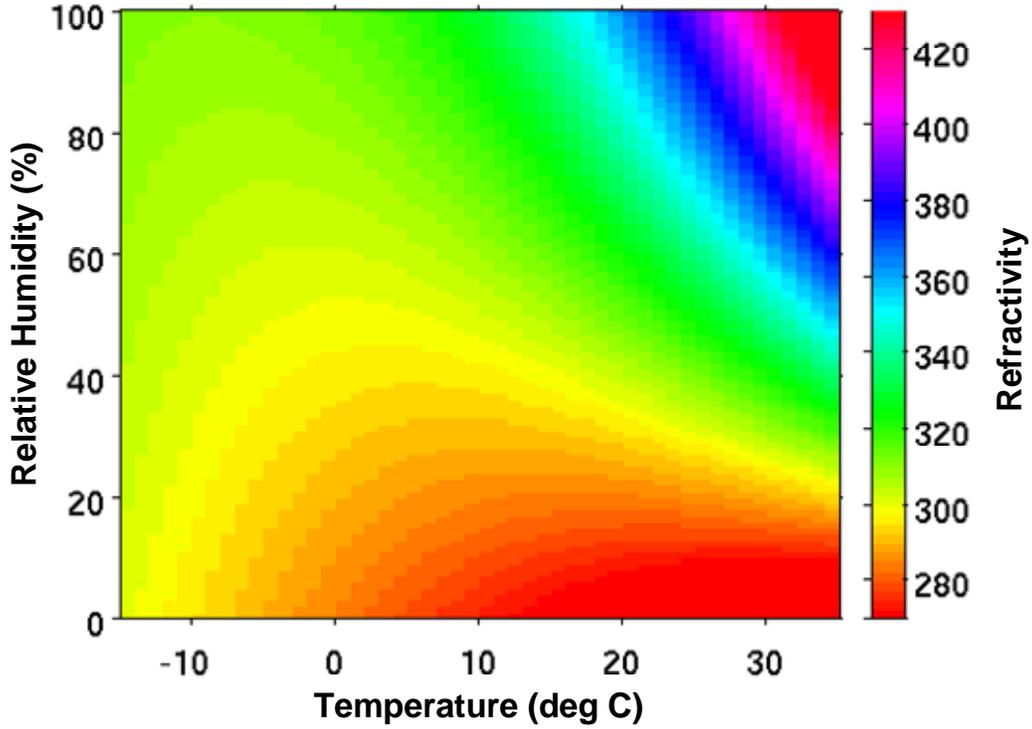
Figure 1. Dependence of refractivity on temperature and relative humidity. Pressure is fixed at 1000 hPa.

Since an ideal target would have a slowly varying phase with no randomly fluctuating component at short time scales, we can use the time coherence of the phase field as a measure of reliability. The coherence can be computed as the lag-1 autocorrelation of the phase time series. Preferably these coherence values are then averaged over a period with significant winds and no weather, so that nonstationary targets are exposed as such, to yield

$$Coh(r) = \frac{1}{M-1} \left| \sum_{k=1}^{M-1} e^{j[\phi(r,t_{k+1}) - \phi(r,t_k)]} \right| , \qquad (7)$$

where M is the number of time series data points used in the calculation.

Another source of contamination is sidelobe clutter. In other words, ground target signal that appears to come from a certain radial direction may, in fact, be coming from an antenna beam sidelobe pointing at another direction. Because ground targets can have extremely large radar cross sections, sidelobe clutter is a serious issue. Fabry (2004) compares the reflectivity of each target to others at all

5

azimuths in the same range gate and marks it as sidelobe clutter if it is more than a threshold value (e.g., 60 dB) below the sum of all other target reflectivities. We felt that this was a somewhat ad hoc procedure, so instead we utilized the fact that azimuthal sidelobe clutter has nonzero Doppler shift due to the radial motion between the feedhorn, which is offset from the axis of antenna rotation, and the stationary target (Rinehart 1991). The target reliability index was computed as

$$RI(r) = Coh(r) \max\left[0, 1 - \frac{1}{v_{Lim}} \left| \frac{1}{M} \sum_{k=1}^{M} v(r,t_k) \right| \right] , \tag{8}$$

where v is the radial velocity and $v_{Lim} = 1 \text{ m s}^{-1}$. In this way the reliability index is penalized if the average absolute velocity value deviates from zero.

Although the static reliability index should pick out the range-azimuth cells containing good targets, moving targets (aircraft, birds, cars, insect swarms, weather) can drift in and out of these gates. To help screen out such interference, a dynamic quality index is computed for each scan. Fabry (2004) uses the signal-to-noise ratio (SNR), radial velocity, and Doppler spectral width for this purpose. We elect to use the radial velocity and signal quality index (SQI), which is the ratio of the absolute value of the lag-1 autocorrelation to the lag-0 autocorrelation, a measure of the Doppler coherence of the signal. The quality index is computed as

$$QI(r,t) = \min\left[\max\left(0, 1 - \frac{|v(r,t)|}{v_{Lim}} \right), \max\left(0, \frac{\min(1, SQI(r,t)) - SQI_{Lim}}{1 - SQI_{Lim}} \right) \right] , \tag{9}$$

where $SQI_{Lim} = 0.8$. The quality index is maximum (one) when the velocity is zero and the SQI is one. Deviations from these values decrease the quality index. Finally, (8) and (9) are combined to produce the weighting function

$$WF(r,t) = \min\left[RI(r), QI(r,t) \right] . \tag{10}$$

6

Let us now go through the procedure for computing the refractivity change field, step by step. The first two steps are performed off-line and the results are stored for use during real-time operations.

1. Average a series of phase maps to generate a reference field ϕ_{ref}. Ideally, this should be done when the atmosphere is clear of weather and the refractivity is constant throughout the observational domain.

2. Generate the reliability index field as outlined above.

3. Generate phase field ϕ by averaging phase values over each dwell (radial).

4. Subtract the reference phase to get $\Delta\phi$. This corresponds to equation (3).

5. Compute the mean range gradient in phase and subtract this from $\Delta\phi$. This step minimizes the difficulties of phase wrapping with range.

6. Smooth the resulting field using the weighting function field given by (10), multiplied by a range-azimuth pyramid function. Censor areas with the total weighting value below a given threshold.

7. Add back the mean phase gradient.

8. Compute ΔN as given by equations (4) and (5).

9. Optionally convert to humidity field via equation (6) if pressure and temperature are known, and the latter is in the appropriate regime.

3. EXPERIMENT DESCRIPTION

For this initial application of the refractivity measurement technique to the ASR-9 WSP, we searched through our archive of in-phase and quadrature (I&Q) data for cases in which there was no radar-visible weather but there was a change in temperature/humidity.

The case that we selected comes from a series of experiments conducted for the Homeland Defense Chemical Biological Umbrella (HDCBU) program that tested the ability of operational weather radars to detect aerosol plumes released from a crop-duster airplane (Troxel et al. 2006). During the Canadian River 1 (CR1) experiment set in the Oklahoma City area, the Academy ASR-9 at the FAA Mike Monroney Aeronautical Center (MMAC) was operating and recorded I&Q data. The particular segment that we used was from the period of April 4, 2003, 15:30 to 17:43 GMT. Figure 2 shows the SNR and radial velocity fields at the beginning of this period. Strong ground clutter echoes are apparent in the SNR plot and corresponding near-zero Doppler values in the velocity plot. There are faint ring-like signatures visible in the SNR field, which are likely due to sidelobe clutter. No weather or clear-air background signal is seen. Although the Program Support Facility (PSF) Terminal Doppler Weather Radar (TDWR) at the MMAC was also recording I&Q data during the CR1 experiment, equipment failure resulted in no data during this particular time period.
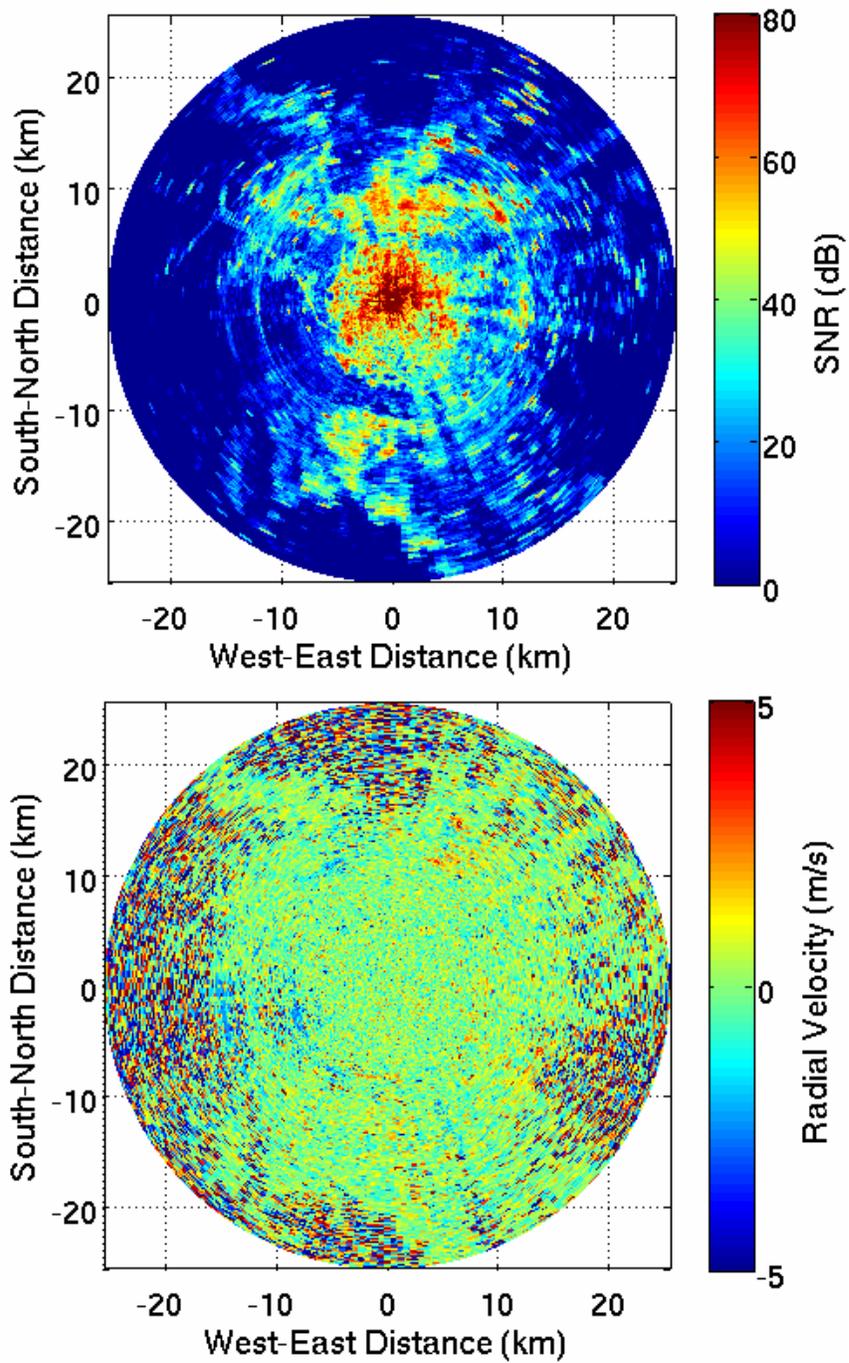
Figure 2. SNR (top) and radial velocity (bottom) fields measured by the Academy ASR-9 WSP at 15:29:48 GMT, April 4, 2003.

10

The system specifications for the ASR-9 are listed in Table 1. The coordinates of the Academy ASR-9 are 35° 24' 4" latitude, –97° 37' 12" longitude, and 409 m above mean sea level (antenna height). Probably the most important figure when comparing the performance of this radar to others in deriving refractivity is system stability, which is largely determined by the phase (rather than amplitude) stability of the system. There is some uncertainty here regarding the number, since specifications given in the design data suggest a value of about 60 dB (transmitter stability of 63 dB, receiver stability of 65 dB, and quantization figure of 71 dB) (Westinghouse 1984), whereas measurements have yielded no more than about 48 dB (Weber and Troxel 1994). We list the more conservative figure in the table.

TABLE 1

MMAC Academy ASR-9 System Characteristics

Frequency	2.7 GHz
Peak Power	1.1 MW
Pulse Length	1 µs
Pulse Repetition Frequency	Dual PRF (1160 Hz average)
Antenna Gain	34 dB
Azimuth Beamwidth	1.4°
Elevation Beamwidth	4.8°
Rotation Rate	12.5 rpm
Range Gate Spacing	116 m
Azimuthal Resolution	1.4°
Sensitivity	1 m^2 @ 111 km
System Stability	48 dB

Figure 3 shows the one-way elevation patterns of the antenna. For this study, we only used the data from the low beam in order to have maximum sensitivity near the ground. The radar was in linear-polarization transmission mode. In this mode, the WSP channel provided valid low-beam data out to 222 gates (26 km). Low-beam data from a 360° scan were available every 12 s. More information about WSP data can be found in a report by Weber (2002).
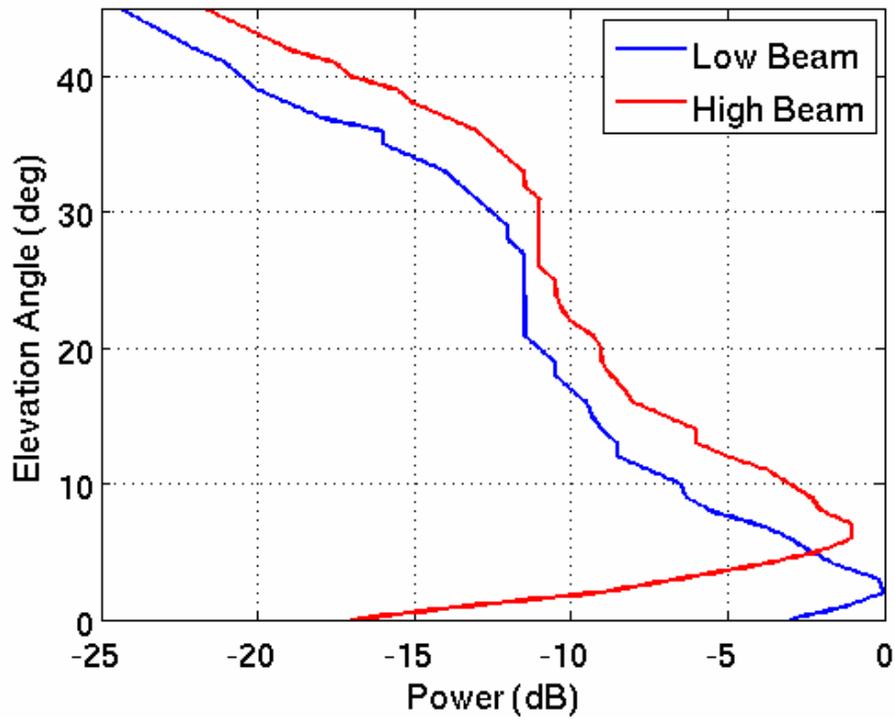
Figure 3. ASR-9 one-way antenna elevation beam patterns.

During the experiment, the wind was blowing from the northwest at about 7 m s^{-1}. Twenty-minute resolution meteorological ground station data from the Max Westheimer Airport in Norman, Oklahoma, were monitored and recorded during CR1 (Figure 4). This station is 22 km southeast of the Academy ASR-9. The synoptic pattern for April 4, 2003 at 12:00 GMT showed the Norman, OK, area to be in light northwest surface flow behind a surface boundary set up about 200 km to the southeast that was active with convective weather. The leading edge of the trailing mid- and upper-level trough was located over north-central Oklahoma around this time. The trough drifted southeastward with time and was south of the Norman area by 00:00 GMT April 5, 2003. In Figure 4, a surface feature is observed between 15:00 and 16:00 GMT with a triplet of a temperature drop, relative humidity increase, and barometric pressure rise. This was likely a response to passage of the trough at higher levels. Analysis of the Oklahoma City (KTLX) WSR-88D radar returns for this time period indicated a small area of moderate reflectivity (25 dBZ) passing very near the radar site. This area dissipated shortly after 16:00 GMT. It is probable that this radar feature was related to instability associated with the trough, and the surface observations were related to evaporative cooling from virga as the feature dissipated (no precipitation was recorded during this time at the surface).
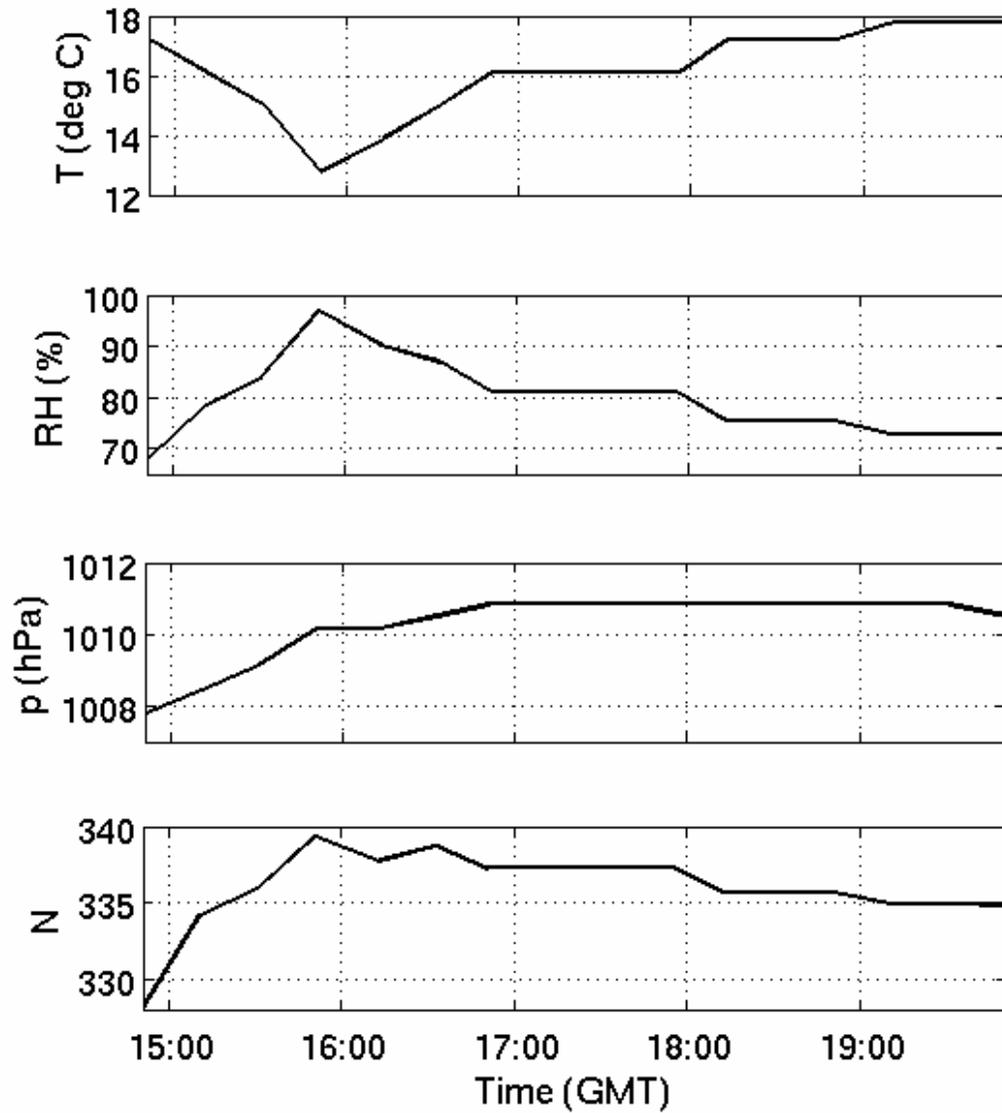
Figure 4. Temperature, relative humidity, and pressure measured at the Max Westheimer Airport in Norman, Oklahoma, on April 4, 2003 at 20-minute intervals. The corresponding refractivity is also computed.

14

4. RESULTS

To generate the reference phase field, we averaged 20 scans over the period 17:39 to 17:43 GMT (Figure 5, top). This period was chosen because the ground-based *in situ* measurements showed slowly varying refractivity during this time (Figure 4). To produce the reliability index map, we used data from 15:30 to 15:50 GMT (100 scans), since the conditions (windy with no weather) were appropriate (Figure 5, bottom). Note that this field is significantly different from the SNR field, indicating that even some of the very strong ground targets were not stable enough for refractivity measurements. Also, the dark ring segments to the southwest showed that sidelobe clutter cells were effectively removed.

The quality index field and the resulting weighting function from the 15:29:48 GMT scan are shown in Figure 6. In some azimuth sectors, very few good targets existed beyond about 15 km in range. This is one of the weaknesses of relying on ground targets—visibility of target is largely dependent on the target height, elevation variation, and the Earth's curvature. The coverage space, therefore, can be rather limited. The top plot in Figure 7 is the raw $\Delta\phi$ field, while the bottom plot is the weighted and smoothed $\Delta\phi$ field, which corresponds to the end of step 7 in the procedure given above. The range-azimuth pyramidal weighting function had a base length of 9 km (for an effective smoothing length of about 4 km) and the threshold weight for censoring was 0.1. Finally, Figure 8 shows the ΔN field.

Although the refractivity estimates were available every 12 s, significant changes in the field were not likely at such short time scales. Therefore, we averaged the results over 5 minutes to generate the time sequence shown in Figure 9. Here we have converted the ΔN values to absolute refractivity using N observed at the Max Westheimer Airport during the time of the reference phase measurement. The location of this airport is indicated by an "X." Although small-scale spatial fluctuations are apparent in the plots, there is a clear decrease in the N field that travels from northwest to southeast, which corresponds to what was observed by the meteorological station at Max Westheimer (Figure 4). This is most apparent in Figure 9c. As noted in the previous section, it is likely that we were observing the recovery phase after the passage of an upper-level trough led to a temporary cooling at lower levels due to virga. The homogenization of the field at the end of the sequence is by definition, since that is the time when the reference phases were computed.

To make an explicit comparison between the radar-derived N estimates and the *in situ* values, we plot the quantities against each other in Figure 10. The trends are quite similar, although the radar estimates are smoother, which could be the result of the extensive spatial smoothing employed in the signal processing.

15
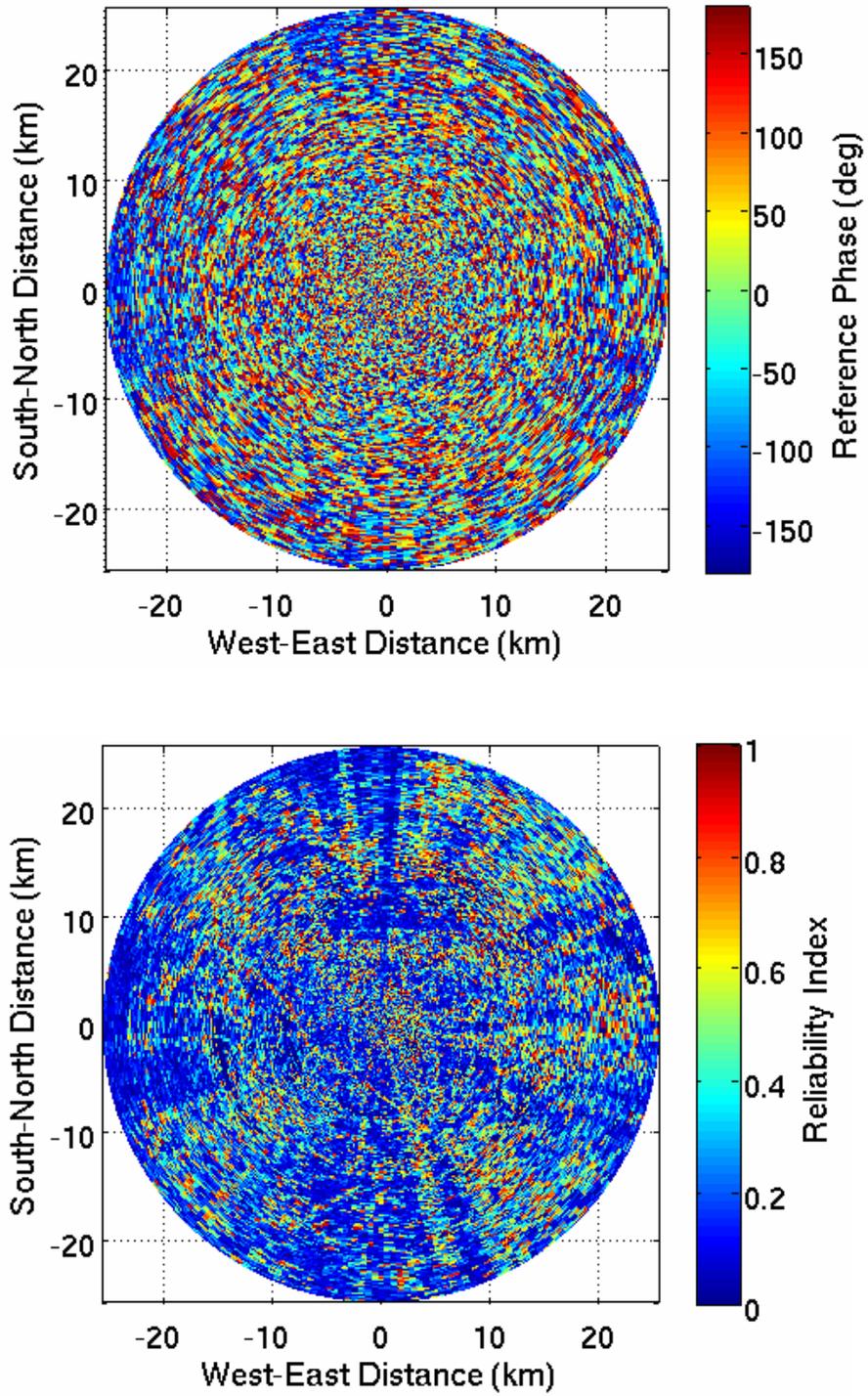
Figure 5. Reference phase (top) and reliability index (bottom) fields.
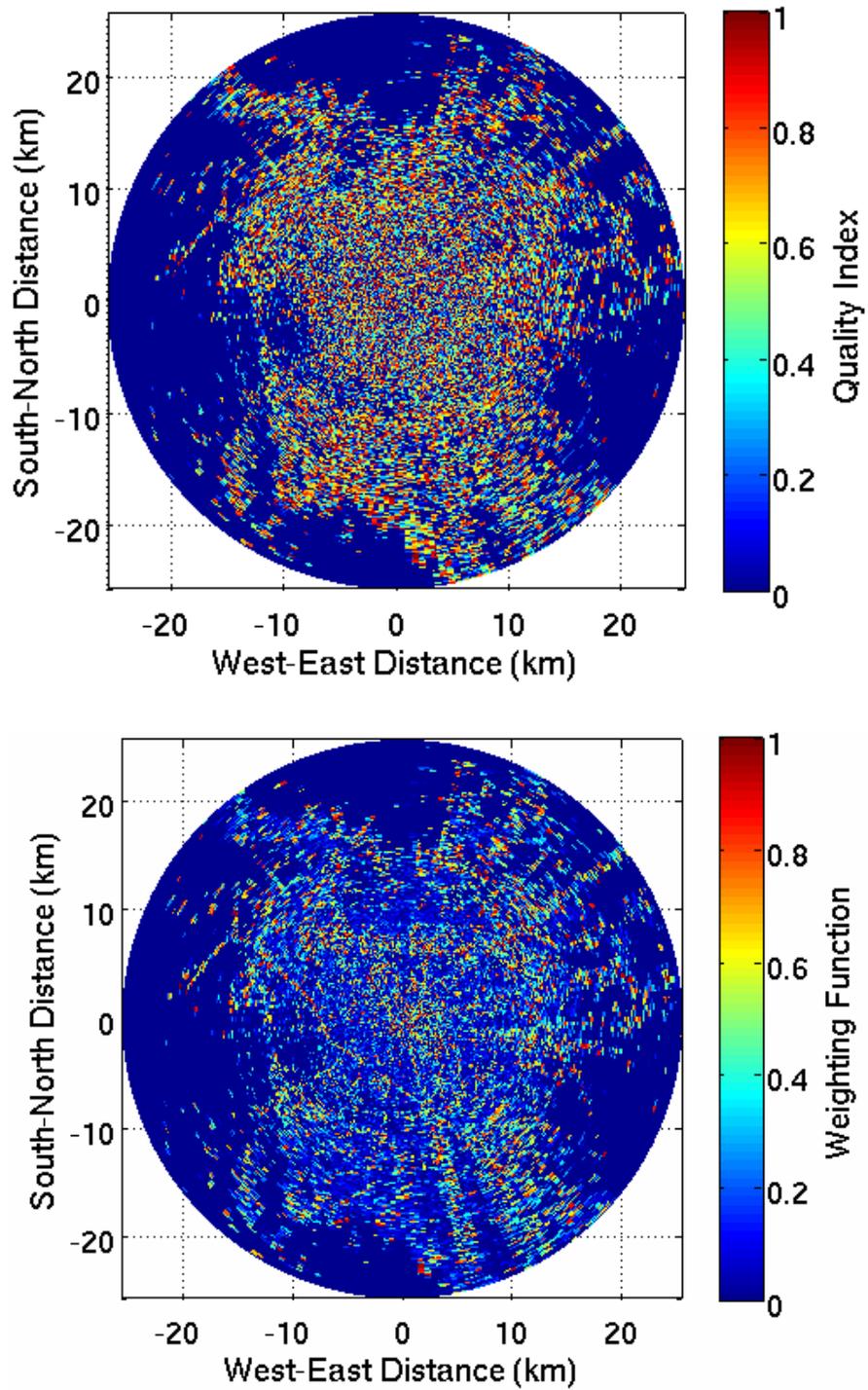
Figure 6. Quality index (top) and weighting value (bottom) fields for the April 4, 2003, 15:29:48 GMT scan.

17
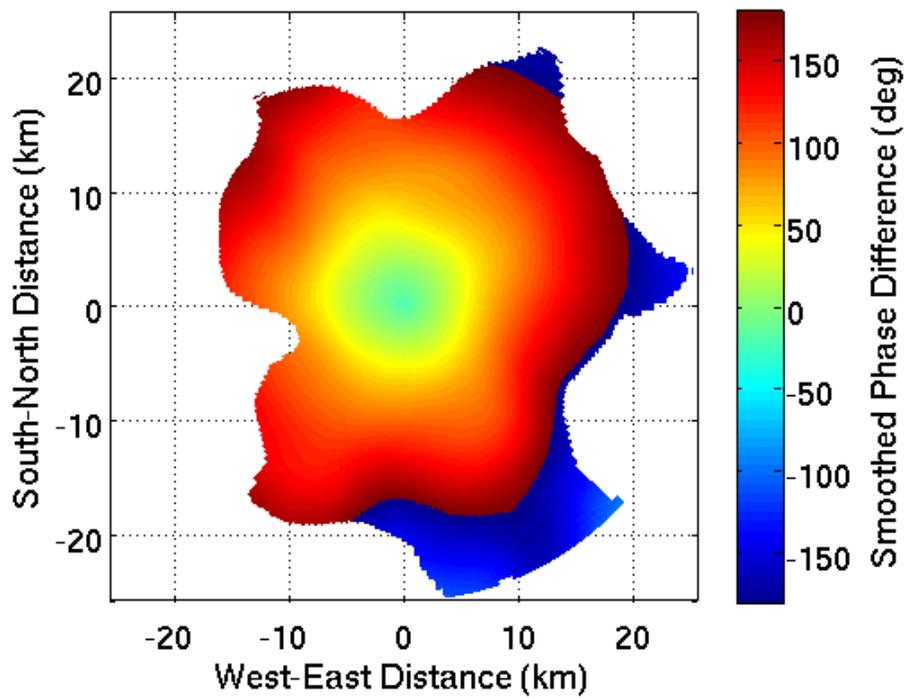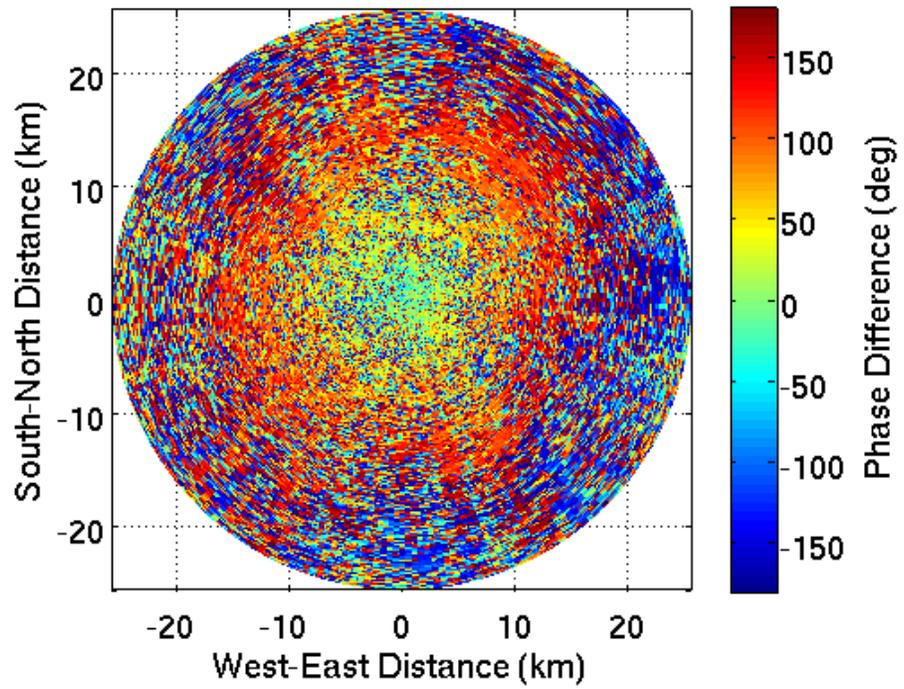
Figure 7. Phase difference (top) and smoothed phase difference (bottom) for the April 4, 2003, 15:29:48 GMT scan.
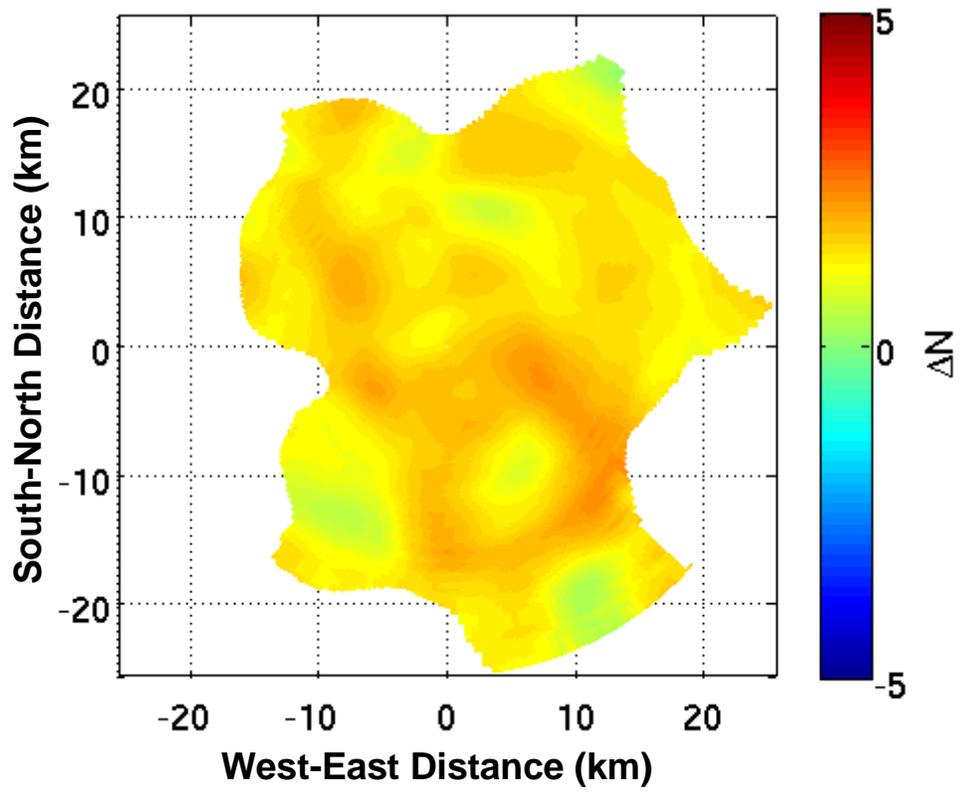
Figure 8. Refractivity change field for the April 4, 2003, 15:29:48 GMT scan.
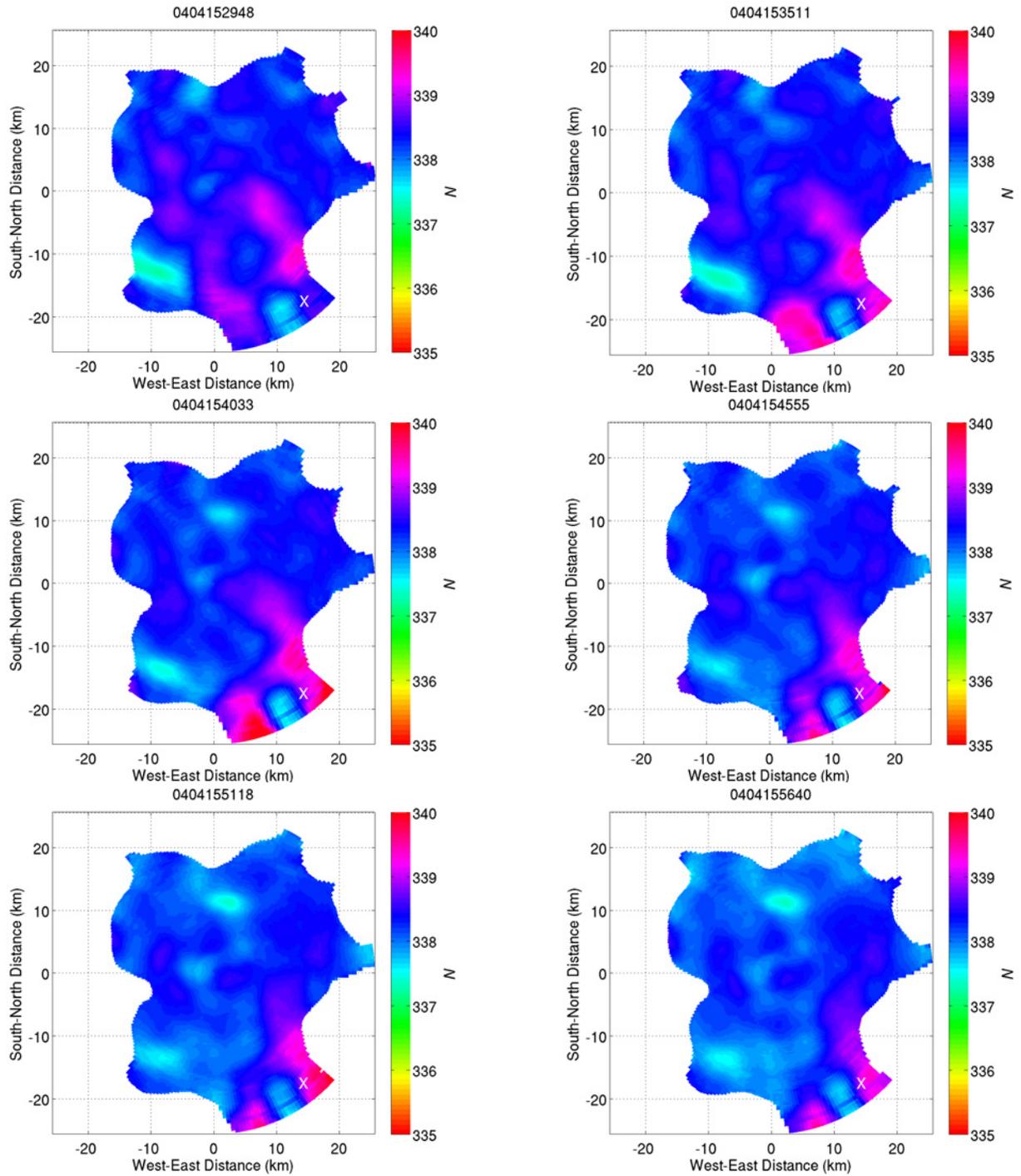
Figure 9a. Time sequence of refractivity field estimates. X marks the location of the Max Westheimer Airport.
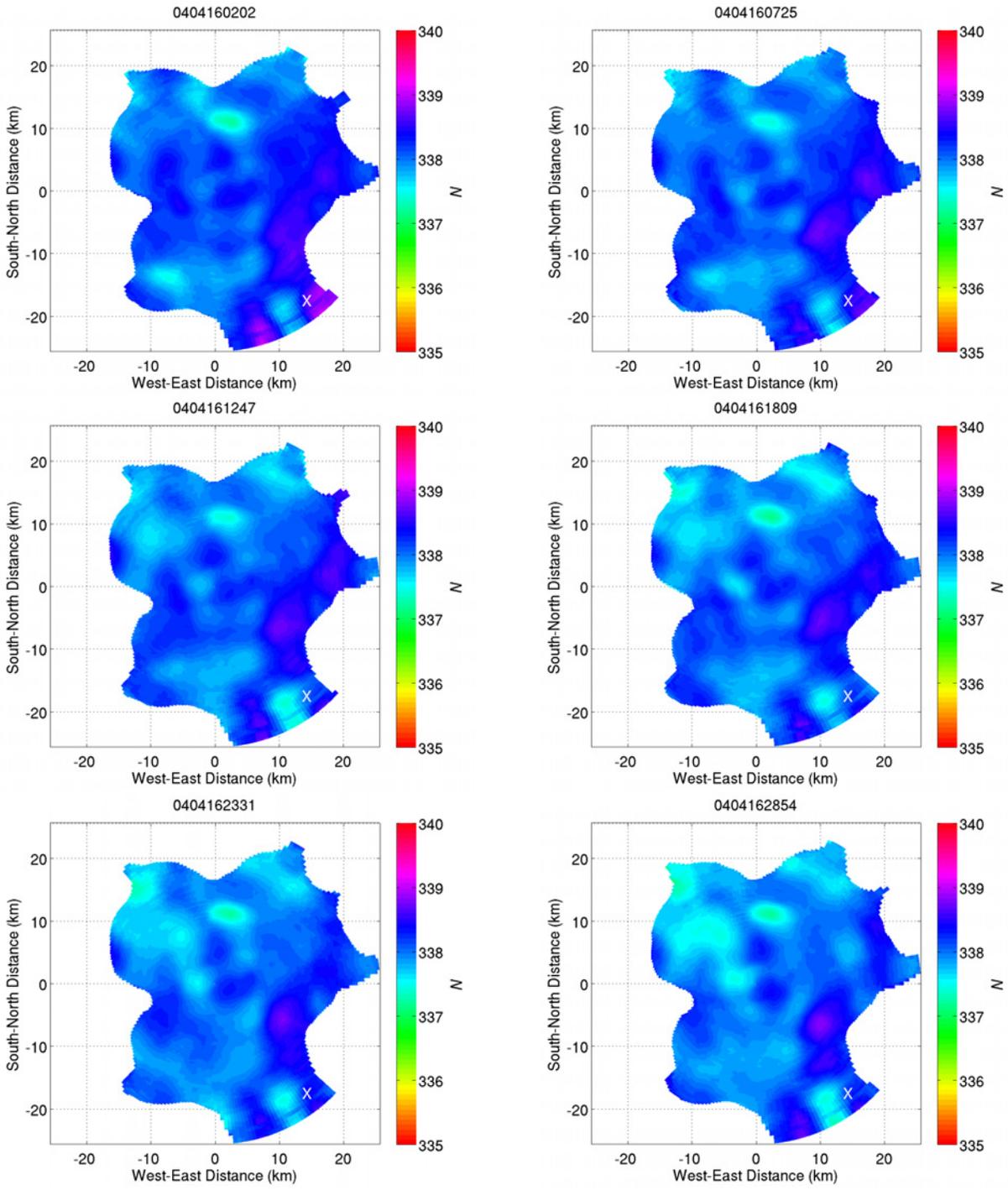
Figure 9b. Same as (a), except at 16:02:02 to 16:28:54 GMT.
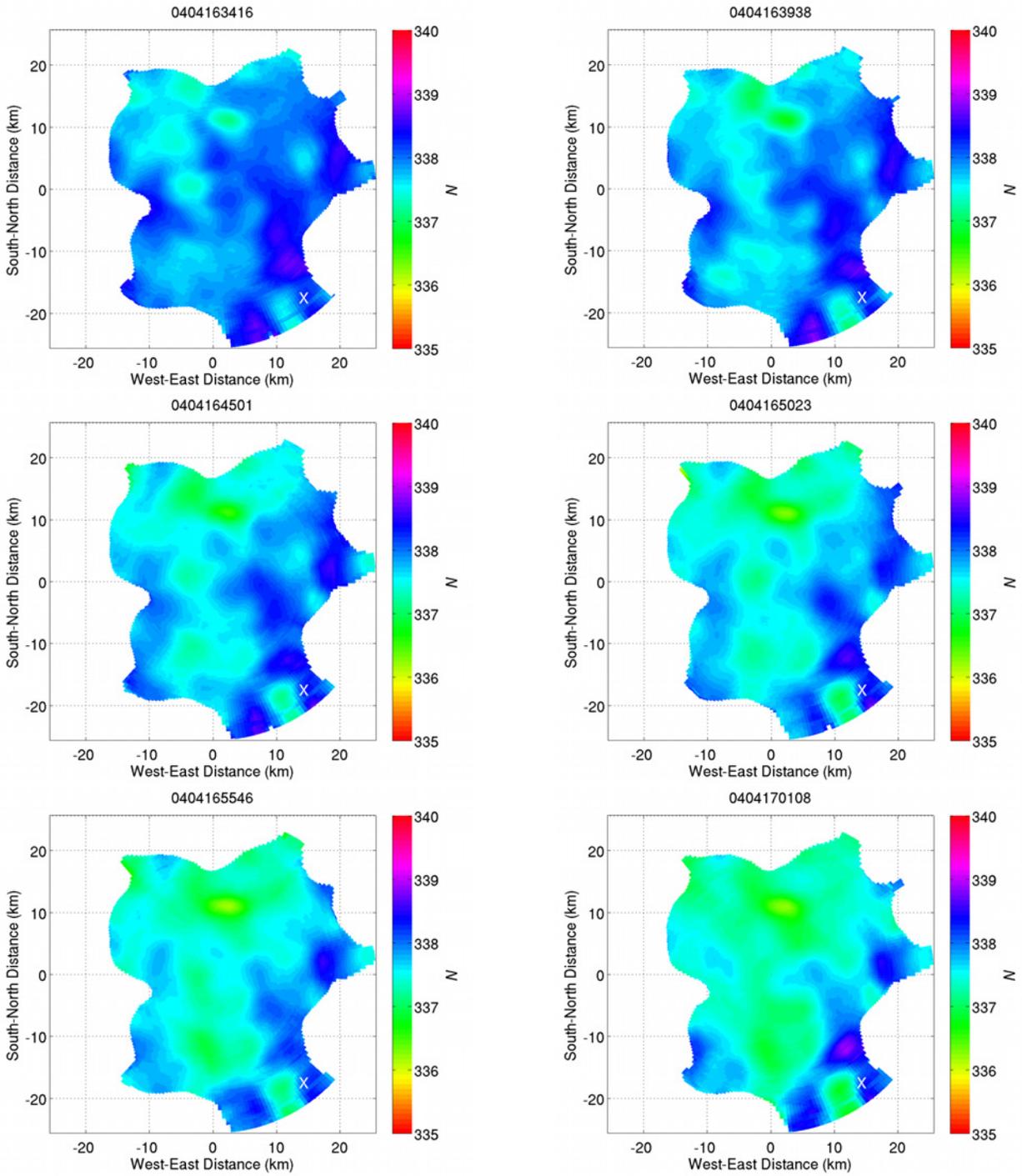
Figure 9c. Same as (a), except at 16:34:16 to 17:01:08 GMT.
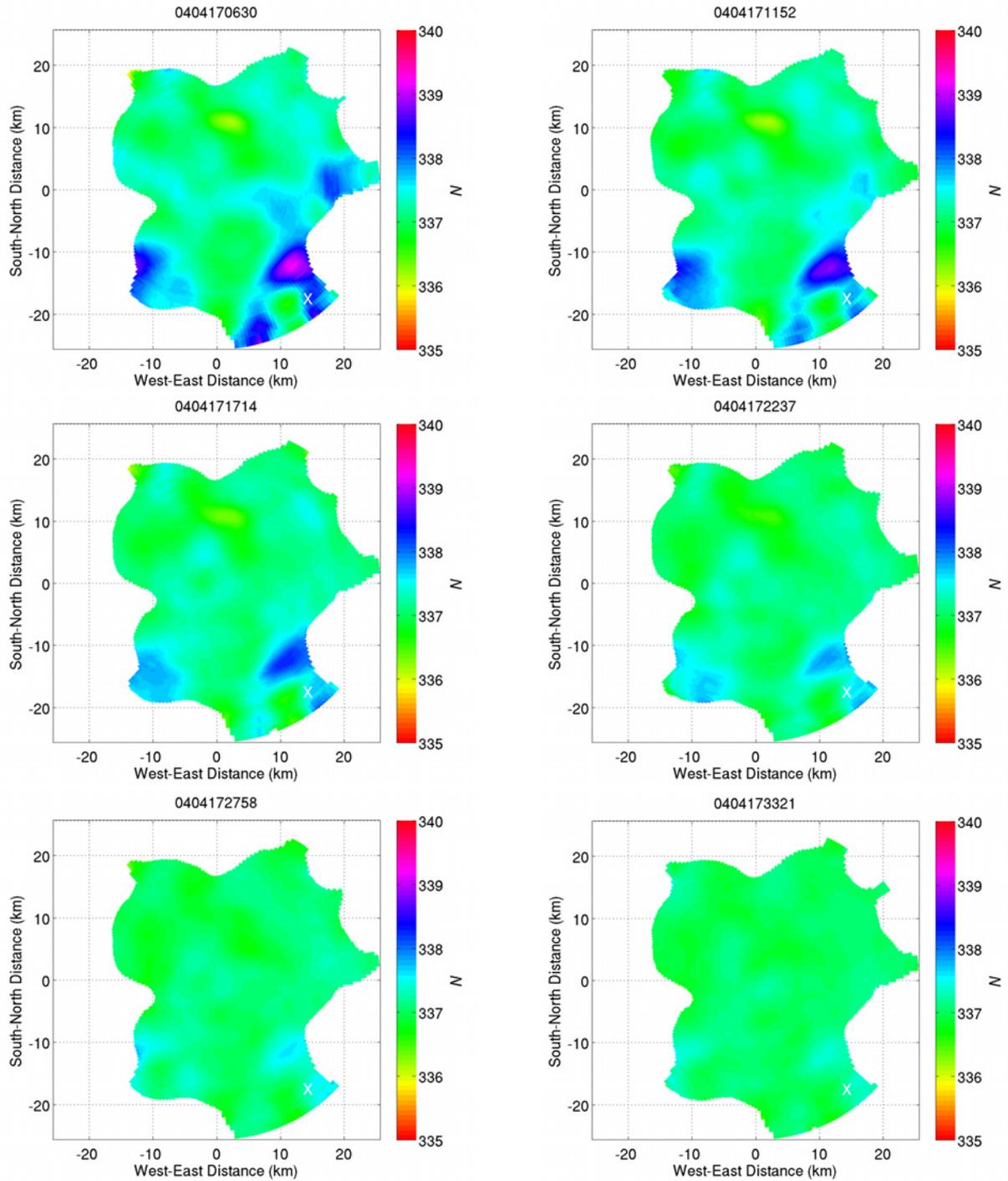
Figure 9d. Same as (a), except at 17:06:30 to 17:33:21 GMT.
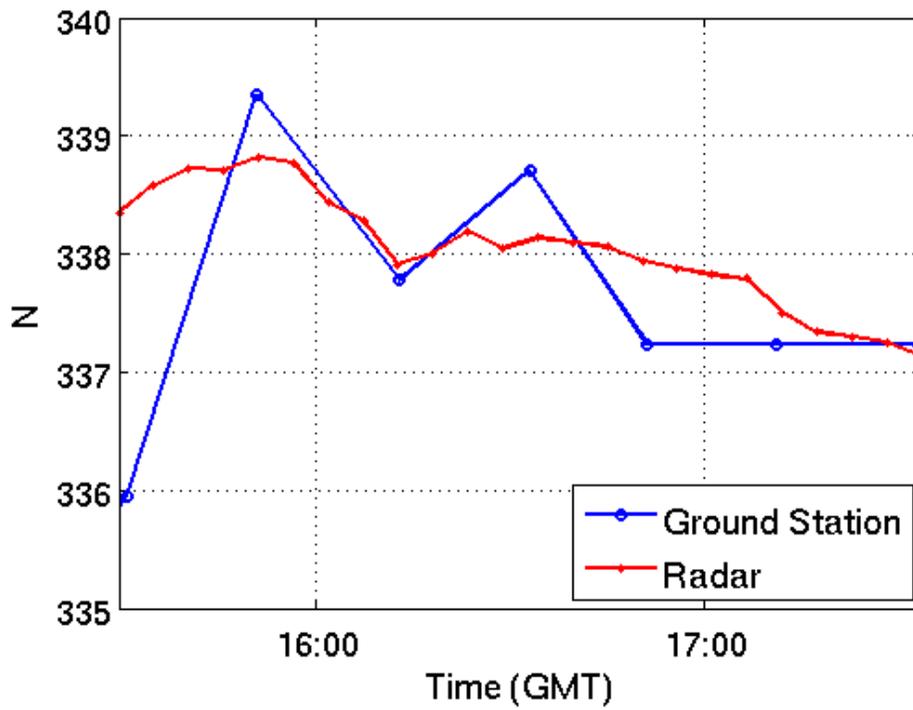
Figure 10. Comparison of refractivity measured at the Max Westheimer Airport meteorological station and ASR-9-derived refractivity estimate at the corresponding range-azimuth coordinates.

5. DISCUSSION

The results from this data analysis showed that ASR-9 WSP data can produce meaningful refractivity estimates. Since the captured event was a fairly gradual change in the refractivity field (rising temperature, falling relative humidity), the plots did not display anything as dramatic as a clearly delineated microburst outflow. In fact, in this case, the specific humidity remained fairly constant, so the refractivity change was mainly due to the temperature variation, not the change in the absolute water vapor content. Unfortunately, the radar was not recording data when a sharp temperature drop occurred about an hour earlier (Figure 4). Future experiments should be planned so that more interesting events are collected on I&Q data.

The results also displayed a significant amount of spatial "lumpiness" despite the extensive spatial smoothing and temporal averaging employed in the data processing. This is characteristic of this technique and is likely due to several issues.

First, if the reference phase measurements are not made during a period of uniform refractivity, then the refractivity estimate map will clearly be distorted relative to the real field. In our initial experiment, we did not have the opportunity to collect radar I&Q data specifically for this purpose. In fact, Figure 4 indicates that the refractivity (measured at a single location in the radar's field of view) was never really constant during the experimental period. Therefore, to further validate this technique for the ASR-9, it is necessary to monitor the refractivity field via a dense network of *in situ* meteorological instruments (e.g., the Oklahoma Mesonet) and record I&Q data when constant refractivity and clear weather are observed.

Second, even if targets are properly selected according to their coherence, changes in the vertical structure of refractivity (not considered in this technique) can affect the results. Anomalous propagation can change the path to target, as well as alter the apparent target shape. Also, if targets are at different heights, the paths to target at the same azimuth do not overlap, making it impossible to separate the contributions from the horizontal and vertical structure of the refractive index. Even a modest difference in target height can generate a significant difference in phase. For example, if the vertical gradient of refractive index is 100 ppm km^{-1}, targets with a 10 m height difference will have phases that differ by 90° at 25 km range on S band (Fabry 2004). As the variance in target height increases, the noise in refractivity estimates increases. It follows, then, that an area with complex terrain would generally produce poorer refractivity estimates compared to an area with flat terrain. Unfortunately, this problem affects dry-site airports, which tend to be located in areas with extensive terrain variance (e.g., Albuquerque).

Third, phase wrapping becomes more rapid as the phase field departs farther from the reference phase field. (Phase wrapping is also more severe for shorter wavelength radars, such as the TDWR at C band.) This by itself is not a problem because dealiasing is straightforward for purely sinusoidal data.

However, noise can lead to incorrect dealiasing, and this problem becomes worse with increased noise and phase wrap. This is the reason for the extensive spatial smoothing that is employed to obtain the results.

The phase instability of the radar system also adds noise to the refractivity estimates. Much of the instability due to the transmitter could be removed by monitoring the phase of the transmitted pulse and using this as a reference for the received signal phase. Up to 65 dB of clutter suppression (i.e., system stability) has been obtained using this method with the TDWR (Cho 2005).

A disadvantage of the ASR-9 compared to pencil-beam radars is that its broad vertical fan beam has an increased chance of intercepting unwanted airborne targets such as birds and aircraft. The azimuthal beamwidth of 1.4° is also wider than other S-band weather radars such as the WSR-88D (0.925°) and the S-band Dual-Polarization (S-Pol) Doppler radar (0.91°), which increases the likelihood of multiple ground targets in the same cell that can complicate phase measurements. The WSP channel also uses an extended coherent processing interval, which further widens the effective azimuthal width of the dwell (Weber 2002).

A major limitation of the radar refractivity technique is the short measurement range. This is a geometrical problem and cannot be remedied. Counterbalancing this is the low cost of implementation. If there is enough spare computational power available in the current signal processing computer, no new hardware would be needed to obtain refractivity estimates. The phase data necessary to the algorithm are already available at the I&Q data stage.

6. CONCLUSION

Despite the lower sensitivity and broader antenna beam of the ASR-9 relative to radars designed specifically for weather surveillance, we were able to show that it could be used to generate refractivity maps from ground target signals. The limited amount of I&Q data collected for other purposes (and general lack of fine-time-resolution temperature and humidity records) did not provide the optimal case for testing this technique, but we were able to obtain reasonable agreement with measurements made at a meteorological station within the radar field of view. Future I&Q data collection should be conducted in coordination with observations from a dense network of meteorological instruments such as the Oklahoma Mesonet. We also need to show that the technique can work well in more complex terrain, such as Albuquerque.

Because refractivity depends on both temperature and humidity, without *a priori* knowledge of the temperature field, absolute humidity values cannot be extracted. If one assumes a smoothly varying temperature field, interpolation across a network of surface meteorological stations [e.g., the Automated Surface Observing System (ASOS) network] could be used to yield temperature data for this purpose. The refractivity field by itself could be used to detect sharp changes that accompany (or lead) aviation hazards such as dry microburst outflows that may not be visible in the radar reflectivity and velocity fields. Such changes are robust against calibration errors, and the application would not require the deconvolution of temperature from humidity.

It would be interesting to test this technique with the TDWR, a more appropriate system than the ASR-9 for measuring refractivity except for its shorter wavelength, which exacerbates the noise-plus-phase-wrap problem. We plan to conduct a preliminary study with data collected by the new TDWR radar data acquisition (RDA) system, which allows I&Q data recording (Cho et al. 2005).

Another potential application platform is the ARSR systems. Since these radars operate at L band, they would be less susceptible to the noise-plus-phase-wrap problem than at S or C band. With 101 operational radars, they would be a significant addition to national coverage if shown to yield good refractivity measurements.

GLOSSARY

ARSR	Air Route Surveillance Radar
ASOS	Automated Surface Observing System
ASR-9	Airport Surveillance Radar-9
CR1	Canadian River 1
FAA	Federal Aviation Administration
GPS	Global Positioning System
I&Q	in-phase and quadrature
MMAC	FAA Mike Monroney Aeronautical Center
RDA	Radar Data Acquisition
S-Pol	S-band Dual-Polarization
TDWR	Terminal Doppler Weather Radar
WSP	Weather Systems Processor
WSR-88D	Weather Surveillance Radar-1988 Doppler

REFERENCES

Bean, B. R. and E. J. Dutton, 1968: *Radio Meteorology. National Bureau of Standards Monogr.*, No. 92, National Bureau of Standards, 435 pp.

Braun, J., 2001: "Validation of a line-of-sight water vapor measurement with GPS." *Radio Sci.*, 36, 459–472.

Cheong, B. L., R. D. Palmer, T.-Y. Yu, and C. Curtis, 2005: "Refractivity measurements from ground clutter using the National Weather Radar Testbed phased array radar." Preprints, *32nd Conf. on Radar Meteorology*, Albuquerque, NM, Amer. Meteor. Soc., http://ams.confex.com/ams/pdfpapers/96318.pdf.

Cho, J. Y. N., G. R. Elkin, and N. G. Parker, 2005: "Enhanced radar data acquisition system and signal processing algorithms for the Terminal Doppler Weather Radar." Preprints, *32nd Conf. on Radar Meteorology*, Albuquerque, NM, Amer. Meteor. Soc., http://ams.confex.com/ams/pdfpapers/96018.pdf.

Evans, J. E. and M. E. Weber, 2000: "Weather radar development and application programs." *Linc. Lab. J.*, 12, 367–382.

Fabry, F., 2004: "Meteorological value of ground target measurements by radar." *J. Atmos. Oceanic Technol.*, 21, 560–573.

Fabry, F., C. Frush, I. Zawadzki, and A. Kilambi, 1997: "On the extraction of near-surface index of refraction using radar phase measurements from ground targets." *J. Atmos. Oceanic Technol.*, 14, 978–987.

Keohan, C., K. Barr, and S. M. Hannon, 2006: "Evaluation of pulsed lidar wind hazard detection at Las Vegas International Airport." Preprints, *12th Conf. on Aviation, Range, and Aerospace Meteorology*, Atlanta, GA, Amer. Meteor. Soc., http://ams.confex.com/ams/pdfpapers/105481.pdf.

Rinehart, R. E., 1991: "Spurious velocities in Doppler radar data caused by a moving antenna feedhorn." *J. Atmos. Oceanic Technol.*, 8, 733–745.

Troxel, S. W., J. Cho, R. Frankel, M. P. Matthews, and J. Shaw, 2006: "C-Band aerosol release detector (CBARD) algorithms description." Project Rep. WXCB-2, MIT Lincoln Laboratory, Lexington, MA, 65 pp.

Weber, M. E., 2002: "ASR-9 weather systems processor (WSP) signal processing algorithms." Project Rep. ATC-255, MIT Lincoln Laboratory, Lexington, MA, 63 pp.

Weber, M. E. and M. L. Stone, 1995: "Low altitude wind shear detection using airport surveillance radars." *IEEE Aerosp. Electron. Syst. Mag.*, 10, 3–9.

Weber, M. E. and S. W. Troxel, 1994: "Assessment of the weather detection capability of an airport surveillance radar with solid-state transmitter." Project Rep. ATC-209, MIT Lincoln Laboratory, Lexington, MA, 71 pp.

Weckwerth, T. M., C. R. Pettet, F. Fabry, S. Park, M. A. LeMone, and J. W. Wilson, 2005: "Radar refractivity retrieval: Validation and application to short-term forecasting." *J. Appl. Meteorol.*, 44, 285–300.

Westinghouse, 1984: *System Design Data for the ASR-9 (Final) in Response to Contract Article I, Item 5b*. Westinghouse Data Item SY002, Westinghouse Electric Corporation, Baltimore, MD, 816 pp.